J Oceanogr (2012) 68:427–437
DOI 10.1007/s10872-012-0107-y

ORIGINAL ARTICLE

Enhancement of biological productivity by internal waves: observations in the summertime in the northern South China Sea

Xiaoju Pan · George T. F. Wong · Fuh-Kwo Shiah · Tung-Yuan Ho

Received: 29 September 2011 / Revised: 20 March 2012 / Accepted: 27 March 2012 / Published online: 19 April 2012

Abstract Streaks of elevated concentrations of surface chlorophyll *a* (Chl_*a*) of various spacing were found to be associated with internal waves in their transmission zone and dissipation zone in the summertime in the deep open northern South China Sea. At an anchored station in the dissipation zone north of the Dongsha Atoll with a water depth of ca. 600 m, undulations of the mixed layer depth with an amplitude of ca. 30 m and a periodicity of ca. 12 h were observed, and they were accompanied by similar undulation in the isotherm and isopleth of the nutrients. These observations are consistent with the enhancement of vertical mixing by internal waves and the resulting transfer of cold, nutrient-rich subsurface water to the surface mixed layer to fuel biological productivity. In the transmission zone and dissipation zone, respectively, the summertime (May–October) average sea surface temperature was 0.5 and 0.8 °C lower and Chl_*a* was 19 and 43 % higher than those in a nearby subregion that was minimally affected by internal waves. The mean net primary productivity was elevated by 15 and 37 %. These results indicate that the enhancement of biological activity by internal waves is not confined to the shallow waters on the shelf. The effect can be detected in all phases of the internal waves although it may be especially prominent in the dissipation zone where mixing between subsurface and surface waters is more effective.

Keywords Internal waves · Phytoplankton · Dongsha Atoll · Northern South China Sea · MODIS · Summertime

1 Introduction

The conventionally recognized supply of nutrients to the euphotic zone by diapycnal mixing has been found to be insufficient for supporting the observed primary productivity in the oligotrophic ocean (McGillicuddy and Robinson 1997). Much effort has been devoted to finding this missing supply. A number of novel mechanisms have been hypothesized, including the actions of eddies (McGillicuddy et al. 1998), propagating planetary waves (Cipollini et al. 2001; Uz et al. 2001), migrating diatom mats (Villareal et al. 1999), tropical cyclones (Lin et al. 2003), and the deposition of volcanic material (Lin et al. 2011). Nonlinear solitary internal waves, which are simply called internal waves in this paper, are another mechanism that may enhance vertical mixing. Potentially, they can increase the supply of nutrients to the euphotic zone and thus biological activity by creating shears and turbulence in the pycnocline (da Silva et al. 2002; Holligan et al. 1985; Lande and Yentsch 1988; Wang et al. 2007; Wilson 2011). Studies on internal waves have focused primarily on the physical rather than biogeochemical aspects (Holligan et al. 1985; Liu et al. 2006). Enhanced biological productivity associated with internal waves has been reported but mostly in the shallow waters, and the effect in the deep waters has not been examined extensively (da Silva et al. 2002; Holligan et al. 1985; Wang et al. 2007; Wilson 2011).

X. Pan and G. T. F. Wong contributed equally to this work.

X. Pan (✉) · G. T. F. Wong (✉) · F.-K. Shiah · T.-Y. Ho
Research Center for Environmental Changes,
Academia Sinica, Taipei, Taiwan
e-mail: xpan@gate.sinica.edu.tw; xpanx001@gmail.com

G. T. F. Wong
Institute of Hydrological and Oceanic Sciences,
National Central University, Jhongli, Taiwan
e-mail: gtfwong@gate.sinica.edu.tw

Some of the internal waves with the largest amplitude (140 m or more) in the world are found in the northern South China Sea (NSCS) (Liu et al. 2006). These waves are generated at the Luzon Strait (Hsu et al. 2000; Liu et al. 2006; Zhao et al. 2004). As they propagate westward into the NSCS, they encounter the Dongsha Atoll on the Dongsha Platform, which has a depth of about 600 m (Fig. 1). South of the Dongsha Atoll, the Dongsha Platform ends abruptly and the water depth increases to over 2000 m. The internal waves reaching this region may propagate through it freely and will not be transformed and dissipated until they reach the shallow waters further west off the east coast of Hainan Island, China (Li et al. 2008; Liu et al. 1998; Zhang et al. 2011). In historical compilations, the internal waves in the NSCS are widely and more evenly spaced in the deep water east and south of the Dongsha Atoll (Fig. 1) (Hsu et al. 2000; Zhao et al. 2004). North of the Dongsha Atoll, the water depth decreases sharply at the shelf edge as it drops to less than 100 m. To the west, there is a series of north–south trending shallow banks along 116°E, the Northern and Southern Vereker Banks, where the water depth decreases abruptly to less than 50 m. The internal waves reaching the north of the Dongsha Atoll are thus trapped between the shelf break and the Dongsha Atoll while they are blocked from free propagation to the west by the Vereker Banks. They may be quickly transformed and even dissipated within this region before they reach the continental shelf even though the water is still several hundred meters deep. This transformation is reflected in the decrease in the spacing of the internal waves in this region (Fig. 1). The dissipation of these waves may result in an effective mixing between the subsurface water and the mixed layer water, and thus an effective supply of nutrients to the mixed layer to fuel biological productivity.

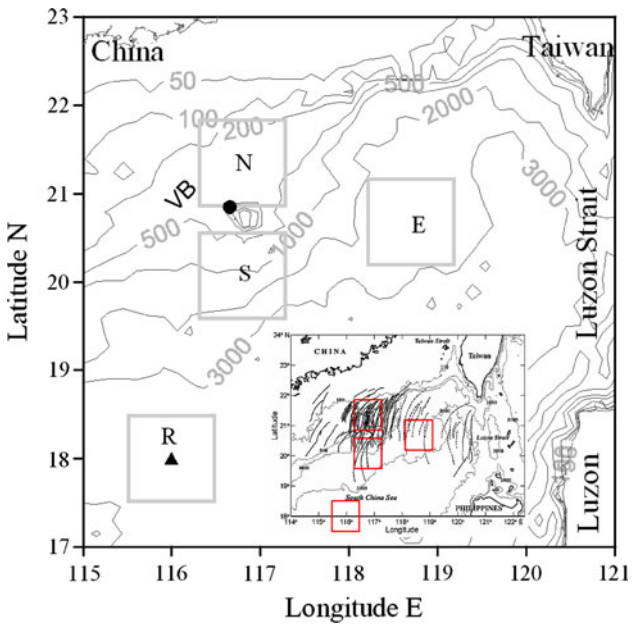

Fig. 1 The bathymetry of the study area. The subregions (1° × 1°) around the Dongsha Atoll from where remotely sensed data were analyzed are shown in the *square boxes*. *N* dissipation zone north of the atoll, *E, S* transmission zones east and south of the atoll, *R* reference site around the SouthEast Asian Time-series Study (SEATS) station. *Filled circle* anchored station (Stn_A) north of the atoll, *filled triangle* SEATS. *VB* North and South Vereker Banks. The historical compilation of the distribution of internal waves in the NSCS between 1995 and 2001 reported by Zhao et al. (2004) is shown in the *inset*

These subenvironments around the Dongsha Atoll provide a unique setting for examining the enhancement of biological productivity by the internal waves in deep waters: the dissipation zone north of the Dongsha Atoll and the transmission zone east and south of the Dongsha Atoll. South of ca. 19°N in the deep NSCS, the occurrence of internal waves is less extensive (Fig. 1; Hsu et al. 2000; Zhao et al. 2004), and this is confirmed by direct observations with mooring arrays (Chang et al. 2010), the estimation of the distribution of the energy flux of internal waves (Lien et al. 2005), and numerical modeling exercises (Zhang et al. 2011). A time-series station, the SouthEast Asian Time-series Study (SEATS) station (Fig. 1), has been established at ca. 18°N and ca. 116°E since 1999 (Wong et al. 2007). This area may serve as a reference site where the effect from internal waves would be minimal as compared to the surrounding area of the Dongsha Atoll (Chang et al. 2010; Hsu et al. 2000; Li et al. 2008; Lien et al. 2005; Zhang et al. 2011; Zhao et al. 2004).

Here, by using remotely sensed data combined with in situ observations, we assess the enhancement of biological productivity in the summertime by the internal waves in the deep waters in the regions around the Dongsha Atoll. Here, the summertime is defined as May through October, covering the southwest monsoonal season (June through September) and the intermonsoonal periods in May and October. The summertime was chosen for two primary reasons. First, the shallow mixed layer and sharp thermocline in the summertime favor the formation of nonlinear solitary internal waves (Qu et al. 2007; Shaw et al. 2009). Second, the stronger wind and surface cooling in the wintertime also enhance vertical mixing and elevate primary production (Tseng et al. 2005) and the effect of internal waves may be masked.

2 Data and methods

2.1 Field observations in the summertime

Field observations in the summertime were made at the SEATS station in regularly scheduled cruises between

Table 1 Summertime (May–October) cruises to the SEATS station from which hydrographic data were used in this study

Years	Periods
1999	19–20 September
2000	23–24 May, 25–27 July, 18–19 October
2001	28–29 June, 3–5 October
2002	2–3 July, 3–4 September
2003	7 August, 4–5 October
2004	5–6 May, 6 August
2005	29–31 July
2006	3–5 July, 20–23 October

1999 and 2006 (Table 1) (Tseng et al. 2005; Wong et al. 2007) and at an anchored station (Stn_A; Fig. 1) north of the Dongsha Atoll on 8–10 June 2010. At each station, the vertical distributions of temperature, salinity, in situ chlorophyll fluorescence, and photosynthetically available radiation (PAR) were recorded repeatedly, typically every 1–3 h for a total period of 6–60 h. Water temperature and salinity were recorded by using a conductivity–temperature–depth (CTD) recorder (SeaBird SBE9/11), while PAR and in situ chlorophyll fluorescence were measured by a Biospherical model QSP-200L or QSR-240 quantum scalar irradiance sensor and a Chelsea AQUA^{tracka} III fluorometer, respectively. The mixed layer depth (MLD) is defined as the depth at which two criteria are satisfied for the first time: the temperature is at least 0.5 °C lower than the surface value and the density gradient is greater than 0.1 kg m^{-4}. The euphotic zone depth (EZD) is the depth at which PAR is reduced to 1 % of the surface value.

In addition, discrete water samples were collected at these stations for the determination of phytoplankton pigments and the major nutrients. Pigment samples were collected by filtering ca. 2 L of seawater through 47-mm GF/F filters. Chlorophyll *a* concentration (Chl_*a*) was determined fluorometrically (Strickland and Parsons 1972) by a Turner 10-AU-005 fluorometer in the samples collected at the SEATS station. Specific pigments were determined by high-performance liquid chromatography (HPLC) (Bidigare et al. 2002) in the samples collected at Stn_A. The concentrations of the sum of nitrate and nitrite (N + N) and soluble reactive phosphate (SRP) were determined by the methods described by Wong et al. (2007; and references therein).

2.2 Satellite imagery

Observations of level-3 monthly products (4 km resolution) from the MODerate Resolution Imaging Spectroradiometer on Aqua (MODIS-Aqua), including Chl_*a* from the standard operational ocean color algorithms and nighttime (4 μm) sea surface temperature (SST) between July 2002 and December 2011, were extracted from the NASA Ocean Color Web (http://oceancolor.gsfc.nasa.gov/). Monthly images (9 km resolution) of net primary production (PP_{eu}) estimated from a Vertically Generalized Production Model (VGPM) (Behrenfeld and Falkowski 1997) on the MODIS-Aqua observations between July 2002 and July 2011 were downloaded from the Ocean Productivity site (http://www.science.oregonstate.edu/ocean.productivity/index.php).

In the subregions north (20.85–21.85°N, 116.32–117.32°E), south (19.57–20.57°N, 116.32–117.32°E), and east (20.18–21.18°N, 118.19–119.19°E) of the Dongsha Atoll and at the reference SEATS site (17.50–18.50°N, 115.50–116.50°E), monthly mean Chl_*a*, SST, and PP_{eu} were estimated in 1° × 1° subareas (designated as subregions N, S, E, and R, respectively; Fig. 1). In these estimations, waters with depths less than 200 m, which are generally defined as the shelf waters, were excluded from analysis in order to make the comparisons among the subregions consistent with the open ocean. Since tropical cyclones may cause significant elevations in Chl_*a* and depressions in SST lasting for several weeks (Lin et al. 2003), data from time periods within 2 months after the passing of tropical cyclones were excluded from analysis. Dates of historical tropical cyclones were taken from the Joint Typhoon Warning Center (JTWC; http://www.usno.navy.mil/JTWC/).

In addition, selected MODIS-Aqua level-0 images on 12 and 13 May 2005 ('A2005132045000.L0_LAC' and 'A2005133053500.L0_LAC') were downloaded from the Ocean Color Web. They were processed to the level-1B Earth View (EV) products and level-2 products of Chl_*a* with a resolution of 250 m per pixel by using the SeaWiFS Data Analysis System software (SeaDAS version 6.2). The level-2 Chl_*a* images were masked by the following flags: land, high light, cloud, stray light, sunglint, shallow water, high sun zenith angle (>70°), and high satellite zenith angle (>60°). The level-1B and level-2 images were then mapped isotropically to 444 pixels per degree of latitude or longitude, approximately equivalent to the resolution of 250 m per pixel, by using SeaDAS.

3 Results and discussion

3.1 Effects of internal waves from in situ observations

The diurnal variations in water temperature, salinity, and in situ chlorophyll fluorescence, as well as the MLD, EZD, and the depth of the deep Chl_*a* fluorescence maximum (DCM), at Stn_A in subregion N in June 2010 and at SEATS in subregion R in July 2006 are shown on Fig. 2. At Stn_A, the MLD varied between 15 and 50 m with an

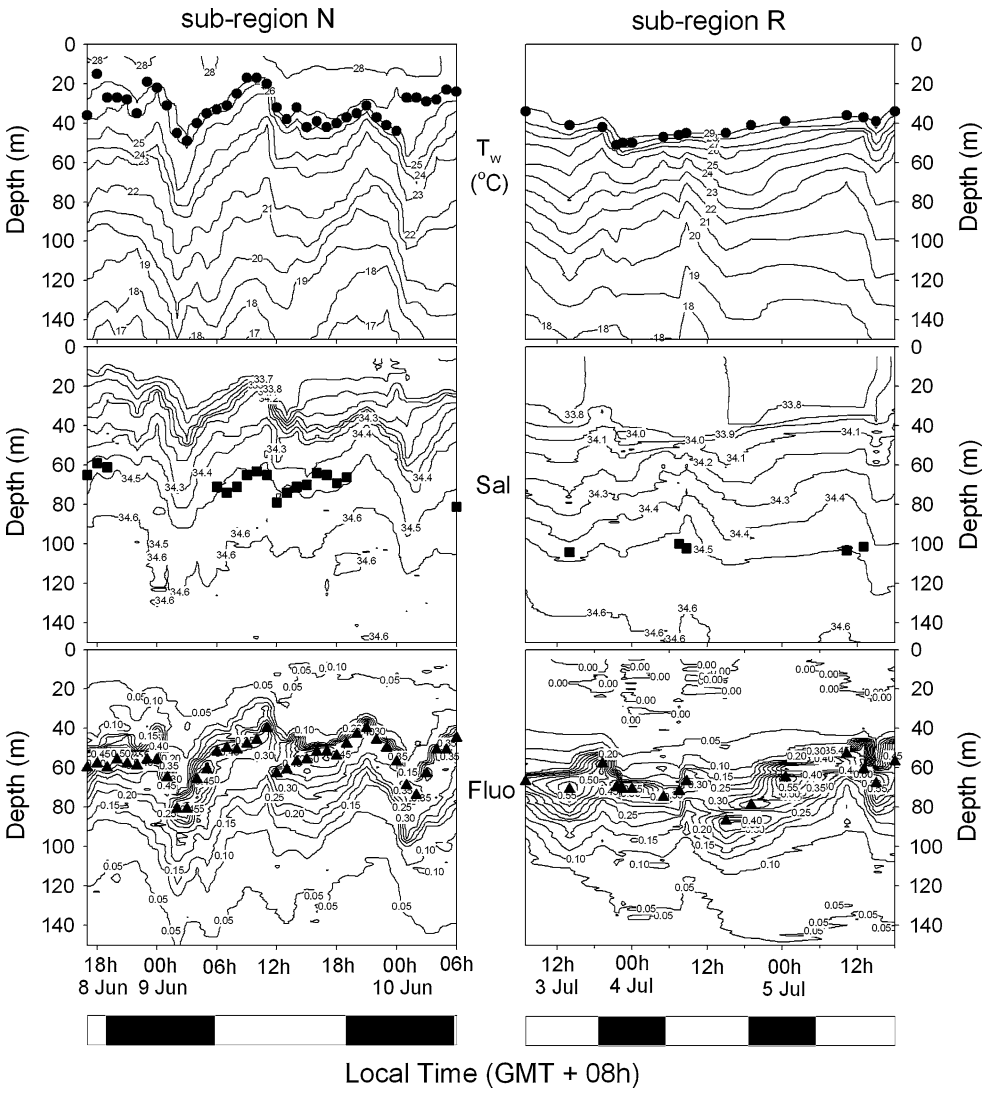

Fig. 2 Diurnal variations in water temperature (T_w), salinity (*Sal*), and chlorophyll *a* (Chl_*a*) fluorescence (*Fluo*) at Stn_A in subregion N (8–10 June 2010) and at the SEATS station in subregion R (3–5 July 2006). *Filled circles* mixed-layer depth (MLD), *filled squares* euphotic zone depth (EZD), *filled triangles* the depth of the deep Chl_*a* fluorescence maximum (DCM). The daytime and nighttime periods are also shown on the *white* and *black bars* below the *x* axes, respectively

average of 32 ± 9 m. It fell approximately along the 26.0 °C-isotherm and the 34.2-isohaline. The MLD oscillated with depth in a regular temporal pattern with an amplitude of about 30 m and a period of 12 h. The periodicity is similar to the reported periodicity of the internal waves in the region (Chang et al. 2010; Lien et al. 2005; Ramp et al. 2004). Correspondingly, the isohalines and isotherms oscillated in depth with amplitudes of about 40 m and periods of 12 h. In contrast, at the SEATS station in subregion R, the MLD ranged between 35 and 50 m with an average of 42 ± 6 m. It fell approximately along the 28 °C-isotherm and the 34.0-isohaline. The temporal variation in the MLD was smaller and it did not follow a semidiurnal pattern closely. Correspondingly, the isohalines and isotherms oscillated in depth only slightly with amplitudes of about 20 m. The period of the oscillation was somewhat irregular, primarily following a diurnal cycle (Chang et al. 2010). All these contrasting behaviors are consistent with an extensive occurrence of internal waves in the form of internal tides in the region north of the Dongsha Atoll and a minimal occurrence, but not necessarily a complete absence, of internal waves at the SEATS site (Chang et al. 2010; Hsu et al. 2000; Liu et al. 2006; Zhang et al. 2011; Zhao et al. 2004, 2008). The EZD varied between 60 and 80 m at Stn_A (average 69 ± 6 m) and stayed approximately constant at around 100 m at the SEATS site (average 102 ± 2 m). These depths were deeper than the corresponding MLD in both subregions. The depth of the DCM oscillated with depth at both Stn_A and the SEATS station. At the SEATS station, the amplitude was 20–30 m. The depth of the DCM was generally deeper during the day and shallower at night, supporting that the variation was caused primarily by the diurnal vertical migration of the phytoplankton in response to the change in light condition (Cullen 1982; Cullen et al. 1983). On the other hand, at Stn_A, the oscillatory amplitude (30–40 m) was larger. The temporal pattern followed those of isotherms and isohalines and was relatively independent

of the light and dark period of the day. This is suggestive of the dominant effect of the internal waves. Thus, while the effect of internal waves at the SEATS station cannot be completely ruled out, it is likely to be much more subdued relative to that at Stn_A.

The diurnal variations in the mean values of water temperature (T_w), N + N, and Chl_*a* determined in the discrete samples and estimated from the in situ fluorescence sensor in the top 50 m (the approximate maximum MLD) at Stn_A in subregion N are shown in Fig. 3. Temperature and N + N followed similar but anti-correlated temporal patterns of regular oscillation in depth with a period of about 12 h. The variations in SRP followed the same pattern as that of N + N and are not discussed here. These behaviors are consistent with the effect of internal waves and similar behaviors have been reported in this region previously (Wang et al. 2007). In general, lower temperatures were associated with elevated concentrations of nutrients ($r = -0.8$), suggesting that the undulation of the bottom of the mixed layer by internal waves brought cooler and nutrient-rich water to the surface mixed layer. The pattern in the temporal variations in the mean Chl_*a* was more complicated. Higher Chl_*a* values were associated with higher concentrations of nutrients ($r = 0.6$) and lower temperatures ($r = -0.7$). Superimposed on this pattern, however, would also be the combined effects of diurnal variation of Chl_*a* (Claustre et al. 1999), the oscillation of the depth of the DCM (da Silva et al. 2002) which was located ca. 20 m below the MLD (Fig. 2a), and a 7- to 8-day delayed response of phytoplankton growth to increases in nutrient concentrations (Wang et al. 2007). Since the latter suite of processes might not occur in phase with the changes in the concentrations of nutrients and water temperature, the resulting temporal pattern in Chl_*a* was more irregular. In contrast, the average temperature, N + N, and Chl_*a* in the top 50 m at the SEATS station showed no obvious temporal pattern of regular oscillation in depth with time (Fig. 3). In comparison to the SEATS station, at Stn_A, on average, temperature was lower by over 2 °C, while N + N and Chl_*a* were higher by over 0.6 μM and 0.2 mg m^{-3}, respectively. These suggest that the occurrence of internal waves may result in significant cooling while the concentrations of nutrients and biological productivity are elevated. Although only the observations at the SEATS station in July 2006 were shown here (Figs. 2, 3), similar temporal patterns, indicating minimal effects from internal waves, were found repeatedly at this time-series station during cruises between 1999 and 2006 (Table 1; data not shown) and from mooring observations (Chang et al. 2010), regardless of the phase of the tide in the spring-neap tidal cycle which may modulate the behavior of internal waves (Ramp et al. 2004). This is consistent with the decreasing occurrence of internal waves from the north to the south and the virtual absence of any evidence of internal waves south of ca. 19°N as indicated in satellite observations (Hsu et al. 2000; Li et al. 2008; Zhao et al. 2004) in the NSCS. Thus, while the subregion R is in the same general vicinity as the other subregions so that they may be under similar prevailing environmental conditions, it is far enough away so that the effect of internal waves may be much reduced as compared to subregions N, S, and E. Subregion R is used in this study as a reference site for deducing the effect of internal waves in this general area.

3.2 Surface expressions of the effects of internal waves in ocean color remote sensing

While the occurrence of internal waves has been detected widely from sea surface roughness in synthetic aperture radar (SAR) images (Hsu et al. 2000; Liu and Hsu 2004; Liu et al. 2006; Zhao et al. 2004, 2008), their imprints in ocean color images have not been studied extensively (da Silva et al. 2002; Wang et al. 2007; Wilson 2011). Although the ocean color images have a lower resolution than the SAR images, e.g., a 250-m resolution by the

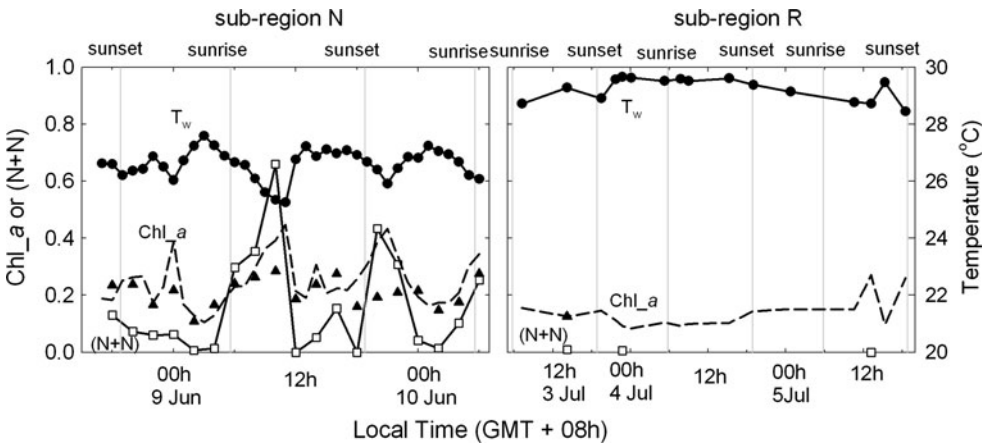

Fig. 3 Diurnal variations in the integrated mean water temperature (T_w), concentration of nitrate + nitrite ($N + N$), and chlorophyll *a* concentration (*Chl_a*) in the top 50 m at Stn_A in subregion N (8–10 June 2010) and at SEATS in subregion R (3–5 July 2006). *Dashed lines* Chl_*a* estimated from in situ fluorescence which had been calibrated against Chl_*a* measured in discrete samples by linear regressions

MODIS-Aqua versus a 25-m resolution by the European Remote Sensing Satellite-2 (ERS-2) SAR sensor, they are able to detect internal waves under cloudless conditions (Jackson 2007; Liu et al. 2006; Zhao et al. 2008). Unlike the SAR images, which have a relatively small coverage (e.g., swath width of about 100 km in image and polarization modes and about 400 km in wide swath and global monitoring modes), the MODIS images have a much larger spatial coverage (2300 km swath) and thus may provide a relatively complete view of internal waves given that the wave crest can be as long as 200 km in the South China Sea (Liu and Hsu 2004).

The Earth View (EV) observations from MODIS-Aqua band-2 (859 nm) at 250 m resolution on 12 and 13 May 2005 are shown in Fig. 4. The north–south trending streaks, visible as dark bands against bright bands of sunglint (Jackson 2007) and located west of the Luzon Strait at ca. 119.7°E (Fig. 4, right panel), most likely represented the surface expressions of internal wave packets in a transmission zone as similar streaks were detected in SAR images in this region and they were attributed to these waves (Liu et al. 2006). East of the Dongsha Atoll at ca. 117.3°E, similar streaks, which were about 150 km long and 1–2 km wide (Fig. 4, left panel), were detected by MODIS-Aqua. However, west of the Dongsha Atoll, the streaks appeared as two bulges and became much more closely spaced (Fig. 4, left panel). The behavior of these streaks was consistent with the known behaviors of internal wave packets in this region as they are generated at the Luzon Strait, propagate westward, and then are split by the Dongsha Atoll into a northern component that undergoes transformation and dissipation and a southern component that continues to propagate freely after refraction (Hsu et al. 2000; Liu and Hsu 2004; Liu et al. 2006; Zhang et al. 2011; Zhao et al. 2004, 2008). Thus, the spacing of successive packets decreased from ca. 50 km northeast of the Dongsha Atoll to 5–10 km north and northwest of the atoll (Fig. 4, left panel). Assuming a wave period of 12 h, the corresponding wave speeds would be 1.2 and 0.1–0.2 m s^{-1}, respectively. These wave speeds are similar to those reported for the internal waves in these subregions (Li et al. 2008; Lien et al. 2005; Liu et al. 2006; Liu and Hsu 2004; Wang et al. 2007).

The corresponding synchronous distributions of surface Chl_*a* are shown in Fig. 5. The streaks that were detected in the Earth View observations (Fig. 4) appeared as similarly spaced streaks of alternately depressed and elevated Chl_*a* (Fig. 5). Propagating internal waves are expected to have such an effect on the distribution of Chl_*a*, and the elevated Chl_*a* strikes most probably resulted from the uplifting of the deep Chl_*a* maximum by the passing internal waves (da Silva et al. 2002). In fact, southeast of the Dongsha Atoll, the presence of the internal waves was more recognizable in the distribution of Chl_*a* (Fig. 5, inset subarea B) than in the Earth View observations (Fig. 4, left panel) as the internal waves became less regularly spaced as a result of their interactions with the Dongsha Atoll and with each other (Zhang et al. 2011; Zhao et al. 2008). Northeast–southwest trending streaks of alternately depressed and elevated Chl_*a* with similar spacing were found in the transmission zone south, southeast and northeast of the Dongsha Atoll (Fig. 4, right panel; Fig. 5, inset subareas B and C) before the waves were significantly modified by their interactions with the atoll. The concentrations of Chl_*a* in the elevation streaks, ca. 0.14 mg m^{-3}, were only moderately higher than the

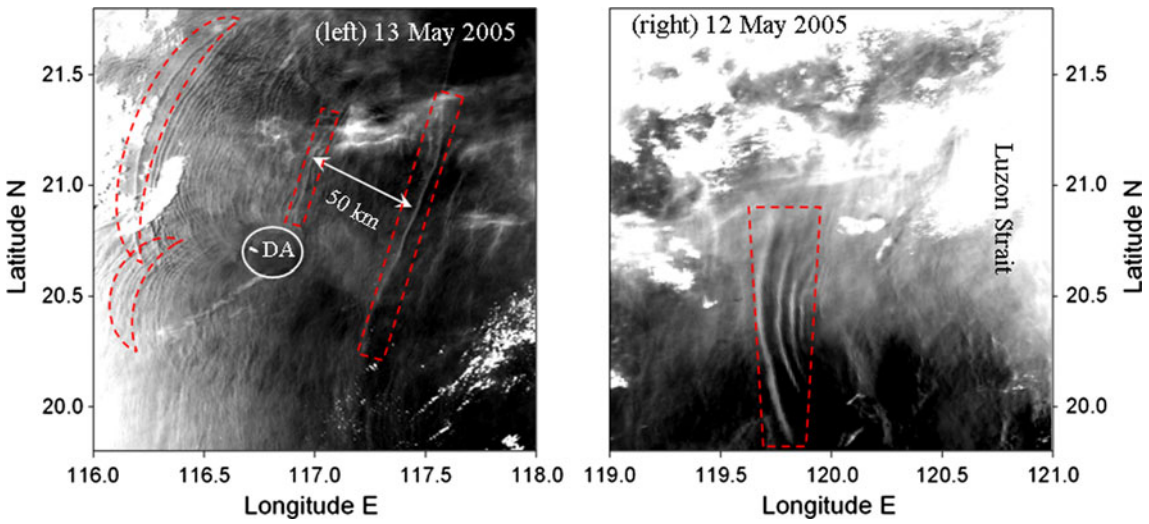

Fig. 4 Earth View (EV) observations from MODIS-Aqua band-2 (859 nm) at 250 m resolution in the areas around the Dongsha Atoll (*DA*) on 13 May 2005 (*left panel*) and west of the Luzon Strait on 12 May 2005 (*right panel*). Selected packets of internal waves, visible as dark bands against bright bands of sunglint, are indicated in envelopes of *dashed lines*

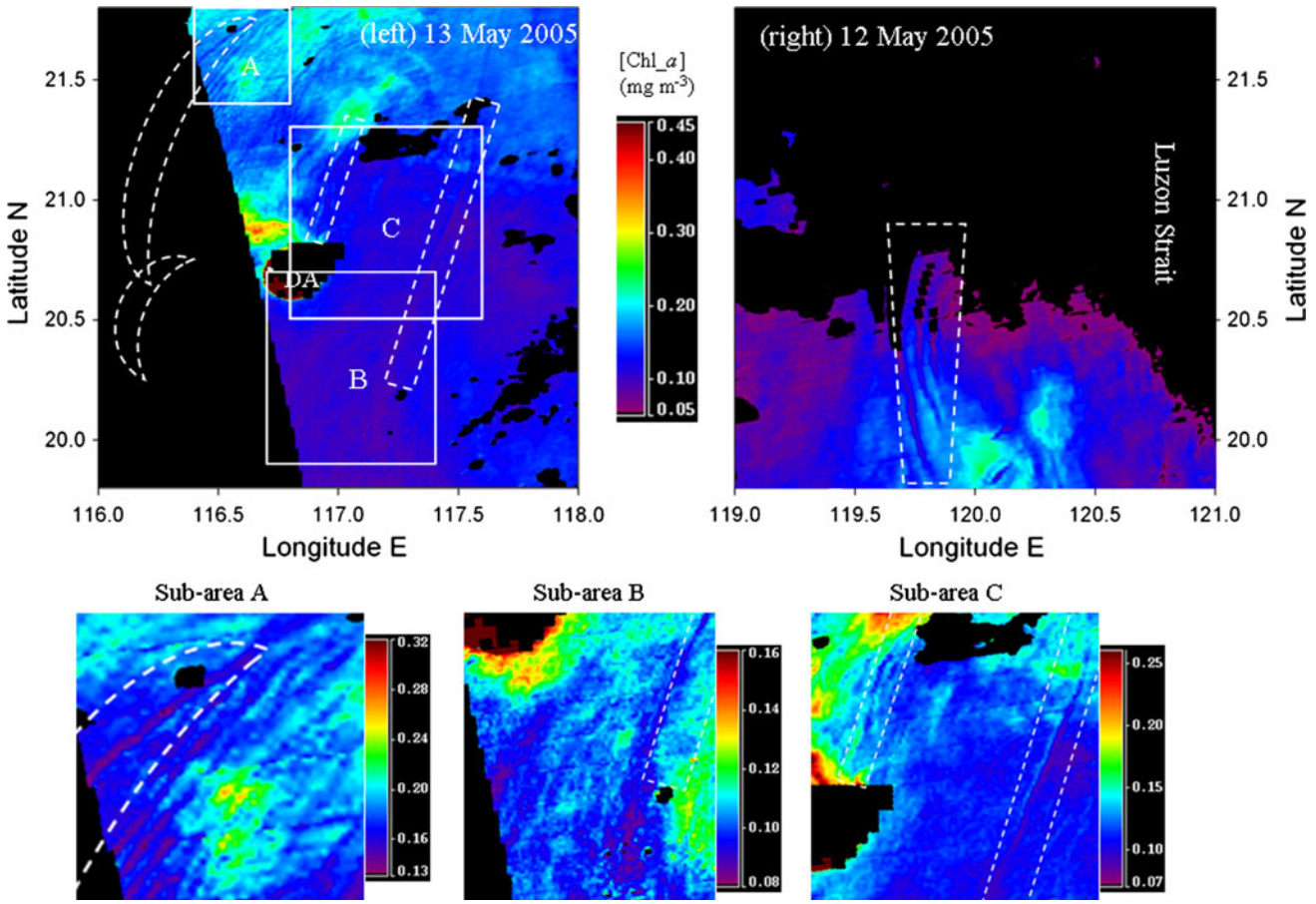

Fig. 5 Corresponding synchronous distributions of Chl_*a* derived from MODIS-Aqua. See more details in Fig. 4. The distributions of Chl_*a* in the *inset* subareas *A*, *B*, and *C* in the *left panel* are rescaled

ambient value of ca. 0.1 mg m^{-3} (Fig. 5). In contrast, in the transformation and dissipation zone north of the Dongsha Atoll, the elevation of Chl_*a* to 0.2–0.4 mg m^{-3} was quite conspicuous (Fig. 5, inset subarea A). Thus, in comparison to the ambient water, Chl_*a* is elevated in the presence of internal waves and it is higher in the transformation and dissipation zone than in the transmission zone.

3.3 Enhancement of biological productivity in the different subregions

The monthly mean Chl_*a*, SST, and PP_{eu} derived from remotely sensed data at the four 1° × 1° subregions (Fig. 1) and the corresponding reported values from direct observation at the SEATS station and surrounding waters (Chen 2005; Tseng et al. 2005; Wong et al. 2007) are shown in Fig. 6. By using the average monthly data at the 1° × 1° subregions, the short-term responses, such as the variations associated with the uplifting of the deep Chl_*a* maximum waters, which occur in minutes to hours, and the delayed response of phytoplankton growth to the increasing nutrients, which takes 7–8 days, should have been largely smoothed out. Therefore, Fig. 6 represents a statistically averaged comparison among the subregions which are affected by the internal waves to a different extent. The remotely sensed estimations in subregion R agree reasonably well with in situ observations. The agreement lends support to the validity of the values estimated from the remotely sensed data. The highest SST and the lowest Chl_*a* and PP_{eu} were found throughout the entire period in the reference subregion R where the effect of the internal waves was minimal. The lowest SST and the highest Chl_*a* and PP_{eu} were found in the dissipation zone of the internal waves in subregion N. The values in the transmission zone in subregions S and E were similar to each other and they fell between those found in subregions N and R. Relative to the subregion R, SST was depressed by 0.5 °C in subregions E and S and 0.8 °C in subregion N, respectively (Table 2). Correspondingly, Chl_*a* was higher by 19 and 43 %, while PP_{eu} was higher by 15 and 37 % (Table 2). These differences relative to subregion R likely represent the minimum effect of the internal waves in the other subregions as the effect of the internal waves in

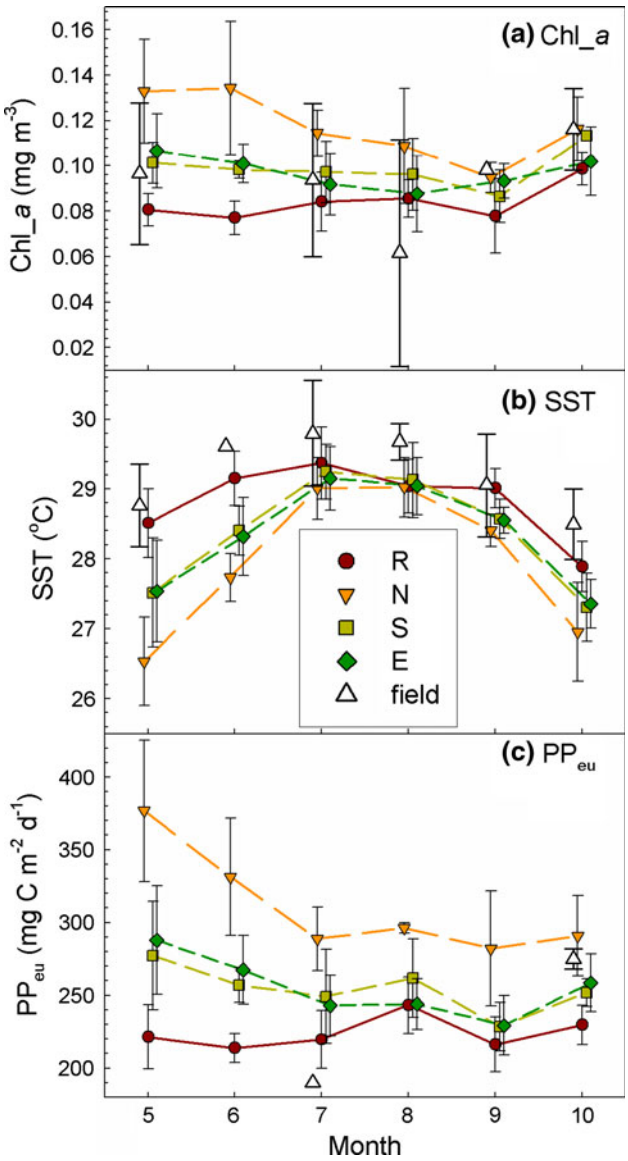

Fig. 6 Climatological (2002–2011) monthly means of **a** Chl_*a*, **b** SST, and **c** primary production (PP_{eu}) in subregions N, S, E, and R between May and October. At each month, data points representing subregions artificially move slightly left or right relative to each other so that they are different from each other. *Open triangles* in situ observations (with standard deviations) of SST and Chl_*a* at SEATS and PP_{eu} adapted from Chen (2005) at locations in the proximity of SEATS

subregion R, while minimal, may not be completely absent (Chang et al. 2010; Lien et al. 2005; Zhang et al. 2011).

3.4 Other possible contributing factors

Aside from internal waves, a number of other processes are known to contribute to the regional variability in the biological productivity in the open NSCS. They include the latitudinal variation in vertical mixing resulting from latitudinal difference in wind stress and solar heat flux (Chu et al. 1997; Qu 2000; Shaw and Chao 1994), the occurrence of mesoscale eddies (Chen et al. 2011; Qu 2000; Shaw and Chao 1994; Wang et al. 2003; Wu and Chiang 2007) and tropical cyclones (Lin et al. 2003), and the inputs of nutrients by atmospheric deposition (Lin et al. 2007, 2011) and mixing with the nutrient-replete shelf water (Gan et al. 2009a, b; Hu et al. 2010). However, these processes are unlikely to be the primary controlling mechanism of the subregional differences reported here.

The subregions N, E, S, and R are located at sufficiently similar latitude, within 3° apart, that their biological productivities should not be controlled by the large-scale latitudinally dependent processes, such as wind stress and solar heat flux. For example, the observed temperature gradient in the region (Chu et al. 1997) account for a temperature difference of only 0–0.1 °C between the subregions N and E or S while the observed difference was 0.1–0.9 °C (Fig. 6b). Since the enhanced supply of nutrients by vertical mixing and the associated elevation in Chl_*a* are associated with the depression of SST, they are also unlikely to be controlled by these large-scale processes. While both mesoscale eddies and tropical cyclones occur commonly in the NSCS (Lin et al. 2003; Wang et al. 2003; Chen et al. 2011), there is no evidence which suggests that their pathways are strongly latitude-specific within a 3° latitudinal band. Similarly, the atmospheric depositional fluxes of nutrients to the NSCS are also not strongly latitude-specific (Lin et al. 2007, 2011). Short-term year-to-year variations are possible. However, since the monthly means estimated here (Fig. 6; Table 2) are averages over 9 years between 2002 and 2011, short-term variations would have been smoothed out.

As to the enhancement of primary production by the input of nutrients from the shelf, if this occurs, the effect should be most prominent in the subregion N which is closest to the shelf. However, the open NSCS is separated from the Northern South China Sea Shelf-sea year round by the South China Sea Warm Current which is located along the shelf edge (Gan et al. 2009a, b; Hu et al. 2010) and this would limit any exchanges between them. Even during the periods of high river discharge in the year (June–July), the fresher surface waters from the shelf are generally confined shoreward within the ca. 100-m isobath (Gan et al. 2009a, 2010). On the other hand, the subregions E and S are located more than 200 km away from the 100-m isobath. Furthermore, the largest depression in SST and elevation in Chl_*a* were found in May (Fig. 6) when the prevailing surface current is westward or southwestward (Chang et al. 2010) so that the offshore eastward intrusion of shelf water onto the open NSCS may be further impeded, suggesting that the observed differences were not caused by the input of nutrients from the shelf. The distribution of surface Chl_*a* in the region supports this

Table 2 Variations in sea surface temperature (SST), chlorophyll *a* concentration (Chl_*a*), and net primary production (PP_{eu}) among the subregions between May and October

Parameters	Subregions			Differences		Ratios	
	R	SE	N	SE–R	N–R	SE/R	N/R
SST (°C)							
Min	27.9	27.3	26.5	−1.0	−2.0	–	–
Max	29.4	29.2	29.0	0.0	−0.1	–	–
Mean	28.8	28.3	27.9	−0.5	−0.8	–	–
SD	0.5	0.7	1.1	0.4	0.7	–	–
Chl_*a* (mg m^{-3})							
Min	0.077	0.087	0.095	0.007	0.018	1.07	1.19
Max	0.099	0.113	0.134	0.024	0.055	1.31	1.73
Mean	0.084	0.098	0.117	0.014	0.033	1.19	1.43
SD	0.008	0.008	0.015	0.007	0.016	0.10	0.22
PP_{eu} (mg C m^{-2} day^{-1})							
Min	214	228	282	16	42	1.07	1.17
Max	243	288	377	63	155	1.29	1.71
Mean	224	255	311	32	82	1.15	1.37
SD	11	18	37	20	45	0.09	0.21

N dissipation zone north of the Dongsha Atoll, *SE* transmission zone south or east of the atoll, *R* reference site at SouthEast Asian Time-series Study (SEATS) station

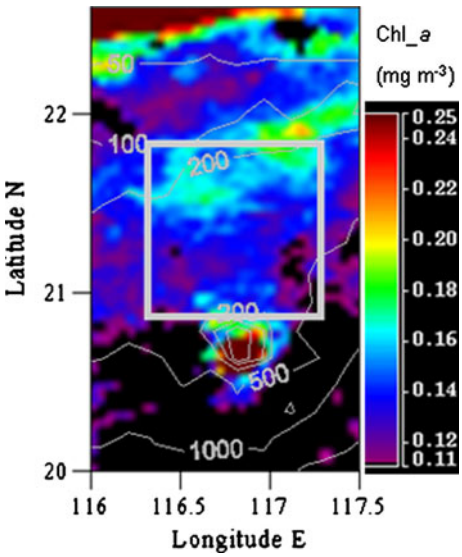

Fig. 7 MODIS-Aqua derived monthly distribution (4 km resolution) of Chl_*a* in May 2005. The subregion N is shown in the *gray box*. A strip of water with low Chl_*a*, approximately between the ca. 50-m isobath and the ca. 100-m isobath, isolates the patch of high Chl_*a* in the subregion N from the high Chl_*a* shelf water

isolation of the water in subregion N from the influence of the seaward intrusions from the shelf as the patch of high Chl_*a* in subregion N is separated from the high concentrations on the shelf by a strip of water with low Chl_*a* concentrations along the shelf edge (e.g., as found in May 2005, Fig. 7).

So, while other processes do contribute to the variations in biological productivity in the NSCS, their contribution to the differences among the subregions, if any, is likely to be secondary. The spatial patterns in the differences are most consistent with the varied effects of internal waves in the subregions.

4 Summary

In the summertime between May and October, the concentrations of Chl_*a* and PP_{eu} are elevated while SST is depressed in the surface mixed layer in the transmission and dissipation zones of the internal waves in the NSCS relative to a subregion that is minimally affected by internal waves. The results are more conspicuous in the dissipation zone than in the transmission zone. These patterns are most consistent with an elevation in biological productivity as a result of the mixing of the cold and nutrient-replete subsurface water with the mixed layer through the action of the internal waves.

Acknowledgments We are grateful to K.-Y. Lee and H.-H. Yang for their determination of nutrients and chlorophyll *a* concentrations in water samples, to the participants in the SouthEast Asian Time-series Study (SEATS) for making their archive data available and to the captains and the crews of R/V Ocean Research I and Ocean Research III for their assistance in sample collection. This work was supported in part by the National Science Council, Taiwan through grants NSC98-2611-M-001-004-MY3 and NSC100-2611-M-001-001 (to Wong) and NSC99-2811-M-001-093 and NSC100-2811-M-

001-095 (to Pan) and by the Academia Sinica through the grants titled "Atmospheric Forcing on Ocean Biogeochemistry (AFOBi)" and "Ocean Acidification: Comparative biogeochemistry in shallow-water tropical coral reef ecosystems in a naturally acidic marine environment" (to Wong).

References

Behrenfeld MJ, Falkowski PG (1997) Photosynthetic rates derived from satellite-based chlorophyll concentration. Limnol Oceanogr 42(l):1–20

Bidigare RR, Van Heukelem L, Trees CC (2002) HPLC phytoplankton pigments: sampling, laboratory methods, and quality assurance procedures. In: Mueller JL, Fargion GS (eds) Ocean optics protocols for satellite ocean color sensor validation, revision 3, vol 2. NASA Goddard Space Flight CenterGreenbelt, Maryland, pp 231–257

Chang YT, Tang TY, Chao SY, Chang MH, Ko DS, Yang YJ, Liang WD, McPhaden MJ (2010) Mooring observations and numerical modeling of thermal structures in the South China Sea. J Geophys Res 115:C10022. doi:10.1029/2010JC006293

Chen YLL (2005) Spatial and seasonal variations of nitrate-based new productivity and primary productivity in the South China Sea. Deep Sea Res (Part I) 52(2):319–340. doi:10.1016/j.dsr.2004.11.001

Chen G, Hou Y, Chu X (2011) Mesoscale eddies in the South China Sea: mean properties, spatiotemporal variability, and impact on thermohaline structure. J Geophys Res 116:C06018. doi:10.1029/2010JC006716

Chu PC, Lu S, Chen Y (1997) Temporal and spatial variabilities of the South China Sea surface temperature anomaly. J Geophys Res 102(C9):20937–20955. doi:10.1029/97JC00982

Cipollini P, Cromwell C, Challenor PG, Raffaglio S (2001) Rossby waves detected in global ocean colour data. Geophys Res Lett 28(2):323–326. doi:10.1029/1999GL011231

Claustre H, Morel A, Babin M, Cailliau C, Marie D, Marty JC, Tailliez D, Vaulot D (1999) Variability in particle attenuation and chlorophyll fluorescence in the tropical Pacific: scales, patterns, and biogeochemical implications. J Geophys Res 104(C2):3401–3422. doi:10.1029/98JC01334

Cullen JJ (1982) The deep chlorophyll maximum: comparing vertical profiles of chlorophyll a. Can J Fish Aquat Sci 39:791–803

Cullen JJ, Stewart E, Renger E, Eppley EW, Winant CD (1983) Vertical motion of the thermocline, nitracline and chlorophyll maximum layers in relation to currents on the Southern California Shelf. J Mar Res 41(2):239–262. doi:10.1357/002224083788520171

da Silva JCB, New AL, Srokosz MA, Smyth TJ (2002) On the observability of internal tidal waves in remotely-sensed ocean colour data. Geophys Res Lett 29(12):1569. doi:10.1029/2001GL013888

Gan J, Li L, Wang D, Guo X (2009a) Interaction of a river plume with coastal upwelling in the northeastern South China Sea. Cont Shelf Res 29:728–740. doi:10.1016/j.csr.2008.12.002

Gan J, Cheung A, Guo X, Li L (2009b) Intensified upwelling over a widened shelf in the northeastern South China Sea. J Geophys Res 114:C09019. doi:10.1029/2007JC004660

Gan J, Lu Z, Dai M, Cheung AYY, Liu H, Harrison P (2010) Biological response to intensified upwelling and to a river plume in the northeastern South China Sea: a modeling study. J Geophys Res 115:C09001. doi:10.1029/2009JC005569

Holligan PM, Pingree RD, Mardell GT (1985) Oceanic solitons, nutrient pulses and phytoplankton growth. Nature 314:348–350

Hsu MK, Liu AK, Liu C (2000) A study of internal waves in the China Seas and Yellow Sea using SAR. Cont Shelf Res 20:389–410

Hu JY, Kawamura H, Li CY, Hong HS, Jiang YW (2010) Review on current and seawater volume transport through the Taiwan Strait. J Oceanogr 66(5):591–610

Jackson C (2007) Internal wave detection using the Moderate Resolution Imaging Spectroradiometer (MODIS). J Geophys Res 112:C11012. doi:10.1029/2007JC004220

Lande R, Yentsch CS (1988) Internal waves, primary production and the compensation depth of marine phytoplankton. J Plankton Res 10(3):565–571

Li X, Zhao Z, Pichel WG (2008) Internal solitary waves in the northwestern South China Sea inferred from satellite images. Geophys Res Lett 35:L13605. doi:10.1029/2008GL034272

Lien RC, Tang TY, Chang MH, D'Asaro EA (2005) Energy of nonlinear internal waves in the South China Sea. Geophys Res Lett 32:L05615. doi:10.1029/2004GL022012

Lin I, Liu WT, Wu CC, Wong GTF, Hu C, Chen Z, Liang WD, Yang Y, Liu KK (2003) New evidence for enhanced ocean primary productivity triggered by tropical cyclone. Geophys Res Lett 30(13):1718. doi:10.1029/2003GL017141

Lin II, Chen JP, Wong GTF, Huang CW, Lien CC (2007) Aerosol input to the South China Sea: results from the Moderate Resolution Imaging Spectro-radiometer, the Quick Scatterometer, and the measurements of pollution in the troposphere sensor. Deep Sea Res (Part II) 54:1589–1601. doi:10.1016/j.dsr2.2007.05.013

Lin II, Hu C, Li YH, Ho TY, Fischer T, Wong GTF, Wu J, Huang CW, Chu DA, Ko DS, Chen JP (2011) Fertilisation potential of volcanic dust in the low nutrient low chlorophyll western North Pacific Subtropical Gyre: satellite evidence and laboratory study. Global Biogeochem Cycle 25:GB1006. doi:10.1029/2009GB003758

Liu AK, Chang YS, Hsu MK, Liang NK (1998) Evolution of nonlinear internal waves in the East and South China Seas. J Geophys Res 103(C4):7995–8008. doi:10.1029/97JC01918

Liu AK, Hsu MK (2004) Internal waves study in the South China Sea using Synthetic Aperture Radar (SAR). Int J Remote Sens 25:1261–1264. doi:10.1080/01431160310001592148

Liu CT, Pinkel R, Hsu MK, Klymak JM, Chien HW, Villanoy C (2006) Nonlinear internal waves from the Luzon Strait. Eos Trans AGU 87(42):449–451

McGillicuddy DJ, Robinson AR (1997) Eddy-induced nutrient supply and new productivity in the Sargasso Sea. Deep Sea Res (Part I) 44:1427–1450

McGillicuddy DJ, Robinson AR, Siegel DA, Jannasch HW, Johnson R, Dickey TD, McNeil J, Michaels AF, Knap AH (1998) Influence of mesoscale eddies on new productivity in the Sargasso Sea. Nature 394:263–265

Qu T (2000) Upper-layer circulation in the South China Sea. J Phys Oceanogr 30:1450–1460. doi:10.1175/1520-0485(2000)030<1450:ULCITS>20CO;2

Qu T, Du Y, Gan J, Wang D (2007) Mean seasonal cycle of isothermal depth in the South China Sea. J Geophys Res 112:C02020. doi:10.1029/2006JC003583

Ramp SR, Tang TY, Duda TF, Lynch JF, Liu AK, Chiu CS, Bahr FL, Kim HR, Yang YJ (2004) Internal solitons in the northeastern South China Sea: part I. Sources and deep water propagation. IEEE J Ocean Eng 29(4):1157–1181. doi:10.1109/JOE.2004.840839

Shaw PT, Chao SY (1994) Surface circulation in the South China Sea. Deep Sea Res (Part I) 41:1663–1683

Shaw PT, Ko DS, Chao SY (2009) Internal solitary waves induced by flow over a ridge: with applications to the northern South China Sea. J Geophys Res 114:C02019. doi:10.1029/2008JC005007

Strickland JDH, Parsons TR (1972) A practical handbook of sea-water analysis, 2nd edn. Fishery Research Board, Ottawa, p 311

Tseng CM, Wong GTF, Lin II, Wu CR, Liu KK (2005) A unique seasonal pattern in phytoplankton biomass in low-latitude waters in the South China Sea. Geophys Res Lett 32:L08608. doi: 10.1029/2004GL022111

Uz BM, Yoder JA, Osychny V (2001) Pumping nutrients to ocean surface waters by the action of propagating planetary waves. Nature 409:597–600

Villareal TA, Pilskain C, Brzezinski M, Lipschultz F, Dennerr M, Gardner GB (1999) Upward transport of oceanic nitrate by migrating diatom mats. Nature 397:423–425

Wang G, Su J, Chu PC (2003) Mesoscale eddies in the South China Sea observed with altimeter data. Geophys Res Lett 30(21):2121. doi:10.1029/2003GL018532

Wang YH, Dai CF, Chen YY (2007) Physical and ecological processes of internal waves on an isolated reef ecosystem in the South China Sea. Geophys Res Lett 34:L18609. doi:10.1029/2007GL030658

Wilson C (2011) Chlorophyll anomalies along the critical latitude at 30°N in the NE Pacific. Geophys Res Lett 38:L15603. doi: 10.1029/2011GL048210

Wong GTF, Tseng CM, Wen LS, Chung SW (2007) Nutrient dynamics and N-anomaly at the SEATS station. Deep Sea Res (Part II) 54:1528–1545. doi:10.1016/j.dsr2.2007.05.011

Wu CR, Chiang TL (2007) Mesoscale eddies in the northern South China Sea. Deep Sea Res (Part II) 54:1575–1588. doi:10.1016/j.dsr2.2007.05.008

Zhang Z, Fringer OB, Ramp SR (2011) Three dimensional, nonhydrostatic numerical simulation of nonlinear internal wave generation and propagation in the South China Sea. J Geophys Res 116:C05022. doi:10.1029/2010JC006424

Zhao Z, Klemas V, Zheng Q, Yan XH (2004) Remote sensing evidence for baroclinic tide origin of internal solitary waves in the northeastern South China Sea. Geophys Res Lett 31:L06302. doi:10.1029/2003GL019077

Zhao Y, Liu AK, Hsus MK (2008) Internal wave refraction observed from sequential satellite images. Int J Remote Sens 29(21): 6381–6390. doi:10.1080/01431160802175520